

Thermally-Induced Microstructural Changes in a Three-Way Automotive Catalyst

CONF-971026

K.L. More, E.A. Kenik, D.W. Coffey, and T.S. Geer, Oak Ridge National Laboratory, Oak Ridge, TN 37831-6064

J. Theis, W. LaBarge and R. Beckmeyer, Delphi Automotive Systems, Flint, MI 48556

ABSTRACT

The use of advanced electron microscopy techniques to characterize both the bulk and near-atomic level microstructural evolution of catalyst materials during different dynamometer/vehicle aging cycles is an integral part of understanding catalyst deactivation. The study described here was undertaken to evaluate thermally-induced microstructural changes which caused the progressive loss of catalyst performance in a three-way automotive catalyst. Several different catalyst processing variables, for example changing the washcoat ceria content, were also evaluated as a function of aging cycle and thermal history. A number of thermally-induced microstructural changes were identified using high resolution electron microscopy techniques that contributed to the deactivation of the catalyst, including sintering of all washcoat constituents, γ -alumina transforming to α -, β -, and δ -alumina, precious metal redistribution, and constituent encapsulation. The data accumulated in this study have been used to correlate microstructural evolution with thermal history and catalyst performance during various aging cycles and to subsequently evaluate different washcoat formulations for increased thermal stability.

INTRODUCTION

In order to optimize the performance of three-way automotive catalysts (TWCs), it is necessary to understand the effect of changes in catalyst composition and microstructure on the lifetime of the catalyst. This is especially important in understanding the microstructural changes contributing to the deactivation of TWCs, which will result in the time-dependent increase in emissions of HC, CO, and NO_x. There are many independent processes that collectively contribute to catalyst deactivation [1, 2], the most important of which are chemical and thermal mechanisms. Chemical deactivation mechanisms primarily consist of constituent poisoning and surface glazing (Zn-, Ca-, and/or P-containing phases) [3, 4], whereas thermal deactivation

will result in microstructural changes in the washcoat constituents, including the precious metals [5, 6]. These thermally-induced microstructural effects include sintering, alloying, particle size changes, phase transformations, and constituent interactions.

In order to distinguish between the different deactivation mechanisms contributing to a particular catalyst's performance, one must document differences in the microstructure of the catalyst before and after engine/dynamometer testing/use. In many instances, the changes in washcoat structure should be evaluated at the atomic level. While there are a plethora of bulk microstructural characterization techniques available, such as X-ray photoelectron spectroscopy and X-ray diffraction, only a few techniques, primarily transmission electron microscopy (TEM), are capable of providing the type of atomic resolution necessary for ultimate catalyst characterization. Although there have been several significant microscopy studies performed on "model" catalyst systems [7,8], there has been only limited work done on actual automotive catalysts [6,9,10], primarily due to the difficulty in preparing representative samples for TEM examination [11]. In order to better understand the effect of aging on the catalyst, it is important to study the intact washcoat structure (as opposed to scraped, thus mixed, powders). Therefore, to preserve washcoat constituent placement in the fresh and aged catalysts, it was necessary to develop a new TEM sample preparation method during the course of this work, which has been described in detail previously [12].

To produce engine-aged samples for characterization, catalysts were aged using different engine/dynamometer schedules. These schedules have been designed to produce catalysts representative of field-aged catalysts but in an accelerated time frame [13,14]. For this study, the particular accelerated engine/dynamometer tests used were designed to cause primarily thermal deactivation. These test-stand aged catalysts were compared to similarly-formulated catalysts retrieved from an actual field test (these results will not be presented here).

The work presented here summarizes the

DISCLAIMER

This report was prepared as an account of work sponsored by an agency of the United States Government. Neither the United States Government nor any agency thereof, nor any of their employees, make any warranty, express or implied, or assumes any legal liability or responsibility for the accuracy, completeness, or usefulness of any information, apparatus, product, or process disclosed, or represents that its use would not infringe privately owned rights. Reference herein to any specific commercial product, process, or service by trade name, trademark, manufacturer, or otherwise does not necessarily constitute or imply its endorsement, recommendation, or favoring by the United States Government or any agency thereof. The views and opinions of authors expressed herein do not necessarily state or reflect those of the United States Government or any agency thereof.

DISCLAIMER

**Portions of this document may be illegible
in electronic image products. Images are
produced from the best available original
document.**

characterization of several different Pt/Rh TWCs to determine thermally-induced microstructural changes which contributed to and/or caused significant loss in catalyst performance and severely degraded catalyst lifetime. These analyses were conducted to elucidate the mechanisms controlling thermal deactivation of catalysts and to relate the microstructural evolution during aging to overall catalyst performance. Some of the work reported here includes complimentary microstructural evaluations for catalysts described in a previous study [15]; here, Theis et al. documented the aged emission performance of a typical TWC formulation having washcoats containing different levels of CeO_2 . It was determined that the catalyst emission performance reached a maximum when the washcoat contained about 40 vol. % ceria; however, no explanations were given for the observed degradation in emission performance with time.

EXPERIMENTAL

The ceramic monolith converters used for this study were 1.4 L in volume. A proprietary process was used to produce alumina/ceria catalyst washcoats with varying ceria levels of 20, 30, 40, 60, and 90 volume %. The washcoated monoliths were post-impregnated with 0.07 troy oz. Pt and 0.007 troy oz. Rh on a bulk basis, resulting in a washcoat concentration of 1.0 and 0.1 wt. %, respectively. An as-produced "fresh" catalyst was examined microstructurally for use as the baseline. This fresh converter contained approximately 28 vol. % ceria.

All the catalysts were aged on 4.3 L V-6 Chevrolet engines. Each converter to be studied was aged on one of three different accelerated test schedules; Rapid Aging Test 'B' for 75 h (RAT(B)75), which represents approximately 50,000 miles for applications with relatively cool exhaust [13], Rapid Aging Test 'A' for 50 h (RAT(A)50), a higher temperature schedule than RAT(B) that represents approximately 50,000 miles of customer driving for applications with higher exhaust temperatures [14], and RAT(A) for 200 h (RAT(A)200), representative of approximately 200,000 miles of customer driving. These aging tests were designed to cause primarily thermal degradation of the catalyst. The results of A/F sweep tests, cold-start FTP tests, and steady state conversion tests for some of the converters examined during the course of this work (converters with different ceria levels) have been presented previously in Ref. 15 and will not be shown again here. For comparison purposes, an actual vehicle-aged converter identical to the "fresh" converter containing ~28 vol. % ceria, was obtained from a test fleet. The particular field-aged converter analyzed in this study was in use for approximately 68,000 miles and still had better performance than the converters aged using the RAT(A)50 schedule.

After aging and performance testing of the converters, extensive microstructural characterization was conducted to evaluate thermally-induced structural changes occurring in the washcoat. Analyses were

conducted on several central core sections from each monolith: 1" below the inlet face (this is where the thermocouples were mounted during the RAT tests), the middle of the monolith, and 1" above the converter outlet face. Metallographic specimens were prepared from each core by (1) cutting a 2 cm X 2 cm X 2 cm sample, (2) vacuum impregnating with a hard epoxy (Ciba Geigy Araldite-GY502 epoxy and Dexter HD3416 hardener mixed in a 10:1 ratio), and (3) mechanical grinding and polishing. These sections were used for "bulk" characterization using techniques such as optical microscopy, electron microprobe analysis (EMPA) and high resolution scanning electron microscopy (SEM). EMPA was conducted using a JEOL 733 Super Probe and the SEM analysis was performed on a Hitachi S-4500 field emission gun (FEG) SEM. Samples for TEM analysis were prepared in two ways, either by scraping washcoat powders from the monolith channels (causing mixing and thus losing all spatial information using this technique) or by cutting thin slices from the embedded metallographic sections described above. The latter type of TEM specimens were prepared such that a hole (the thinnest material is at the edge of the hole) was made directly in the channel corner, as arrowed in Figure 1. The actual TEM specimen (2 mm X 2 mm) was mechanically thinned to about 150 μm , polished, dimpled within the washcoat to a final thickness of ~25 μm , and Ar^+ ion-thinned to perforation. The specimen was mounted on a carbon support ring to make handling easier. These specimens allow for imaging of the washcoat before and after engine testing. TEM was conducted using either an Hitachi HF2000 FEG-TEM operated at 200 kV or a Philips EM400T FEG. The microscopes are equipped with energy dispersive spectrometers (EDS) for chemical analysis of areas $<1\text{nm}$. Scrapped powders from the inlet section were used for X-ray diffraction (XRD) to identify phase changes.

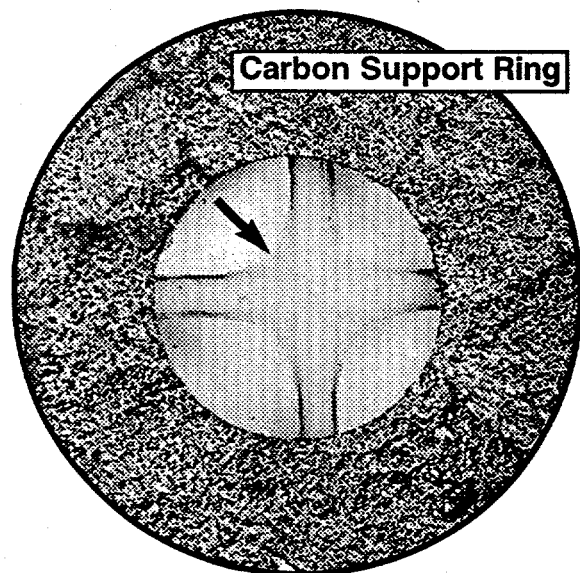


Figure 1. Typical cross section TEM sample showing area of thinned washcoat corner (on cordierite monolith) used for microstructural analysis (corner/fillet arrowed).

RESULTS AND DISCUSSION

The alumina/ceria washcoat in the fresh catalyst was distributed uniformly along the cordierite channels, filling most corners to a depth of approximately 80-100 μm and lining the channel walls at a thickness of about 10-20 μm . A typical region taken from a cross-section through the cordierite substrate is shown in Figure 2 (most of the microstructural analyses conducted in this study were done within the corner regions of the washcoat). Numerous cracks and large bubbles were found within the washcoat corners, as shown in Figure 2, both of which were formed during the drying process. There were few differences observed between the surface of the washcoat and below the surface but for one notable exception; the top 10 μm or so of the washcoat surface was denser than the rest of the washcoat as a result of drying. The general bulk morphology of the "fresh" catalyst washcoat is shown in the SEM image of Figure 3. The washcoat consisted primarily of agglomerated regions ($>1 \mu\text{m}$) of extremely fine-grained γ -alumina particles surrounded by agglomerated regions of fine-grained, acicular ceria (brightly imaging regions in the SEM image). Numerous large-scale pores were also found throughout the washcoat as well as fine-scaled porosity between and within agglomerates of both alumina and ceria. A cross-section TEM image of the fresh catalyst is shown in Figure 4. The extremely small particle sizes of both the γ -alumina ("salt and pepper" features within the labeled agglomerates) and the ceria within the agglomerated regions are clear in this image. Compositional analysis using EDS identified both alumina and ceria and also showed little or no interaction between these different washcoat constituents.

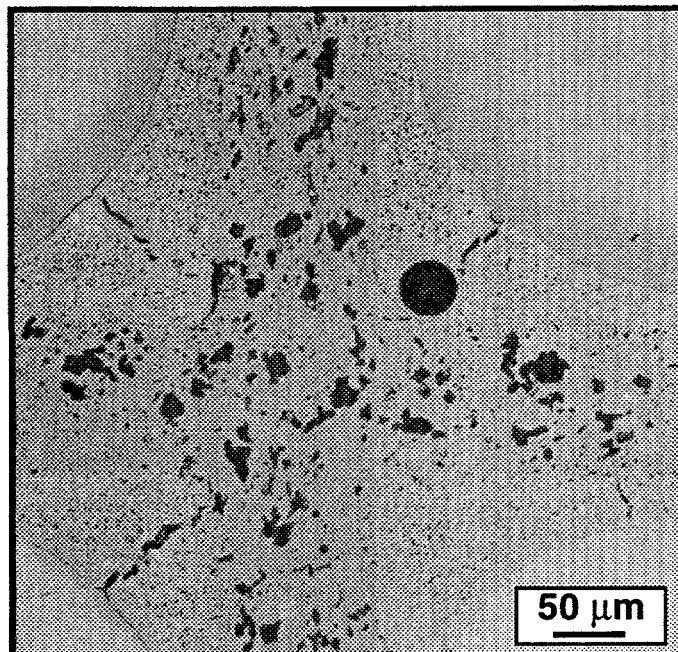


Figure 2. Low magnification optical micrograph showing bulk washcoat morphology on cordierite substrate in the as-processed catalyst.

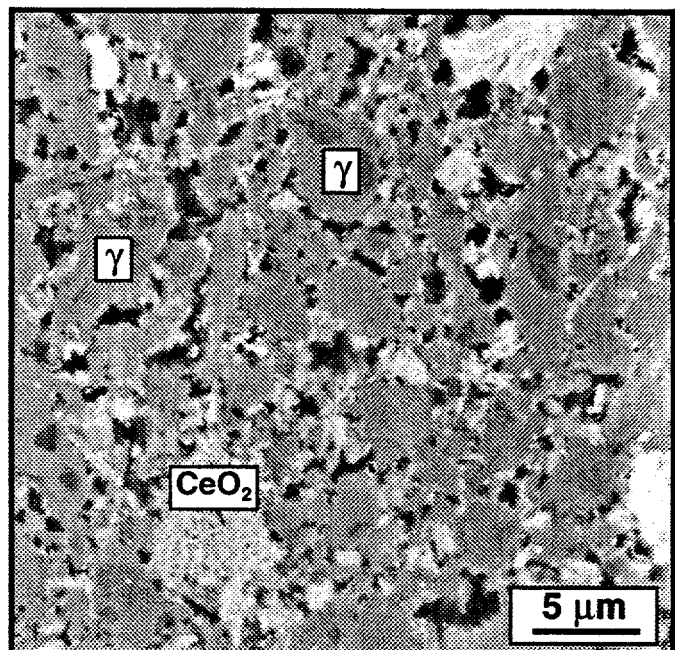


Figure 3. SEM image showing the distribution of alumina and ceria in catalyst washcoat (ceria is brightly imaging phase, pores are black).

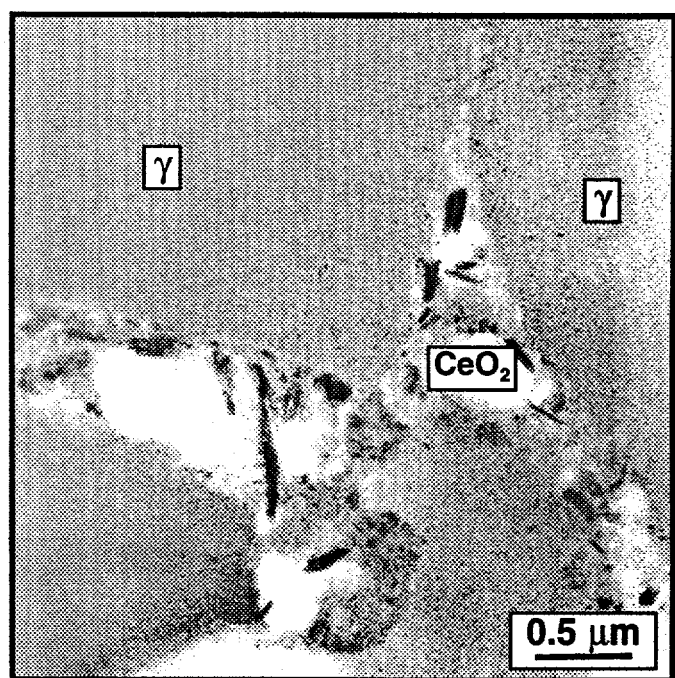


Figure 4. Cross-section TEM image of the fresh catalyst. In the TEM image, the ceria is the dark phase which surrounds the fine-grained γ -alumina agglomerates.

It is necessary to characterize the structure and morphology of all the washcoat constituents in the fresh catalyst, including the γ -alumina, ceria, Pt, and Rh, in order to progressively observe changes occurring as a function of both time (duration of testing) and temperature. TEM analysis showed that only fine-grained γ -alumina was present in the washcoat; no other transition aluminas were identified in the fresh catalyst. This was verified by XRD of scraped washcoat powders.

The γ -alumina particle size was nominally <10 nm. Large γ -alumina agglomerated regions were surrounded by the ceria, as stated previously. The ceria was also present as relatively large, isolated agglomerates. The individual CeO_2 particles were crystalline (but crystallographically defective) and had a needle-like shape. As shown in the TEM image of Figure 5, the CeO_2 particles were characterized as having exposed $<111>$ surface facets. Both the CeO_2 and $\gamma\text{-Al}_2\text{O}_3$ were distributed homogeneously throughout the washcoat, i.e., neither constituent was concentrated at the washcoat surface. EMPA analysis showed that the Pt and Rh concentrations, however, were highest at the washcoat surface. The EMPA was done on the polished cross-section metallographic samples. Line profiles, starting at the washcoat surface to a depth of ~ 80 μm , were done in several washcoat corners, using a beam size of 1 μm and a step size of 0.5 μm . A typical line depth profile of the Pt content in the fresh catalyst is given in Figure 6. Note that the concentration of Pt was significantly greater than 1.0 wt.% at the washcoat surface and much lower below. A similar profile was observed for the Rh in the washcoat but with much lower variations. High resolution TEM and EDS were also used to identify individual Pt or Rh particles. Large area EDS analysis (>1 μm) for very long count times (>1000 s) revealed extremely small amounts of Pt near the washcoat surface, however, no Rh was ever detected via EDS in the TEM. In fact, no individual Pt or Rh particles were found in the as-processed catalyst using either high resolution imaging or high angle dark field (z-contrast) imaging [16] in the scanning transmission electron microscope. This indicates that the Pt and Rh in the washcoat were both likely atomically distributed rather than existing as individual particles or clusters in the fresh catalyst.

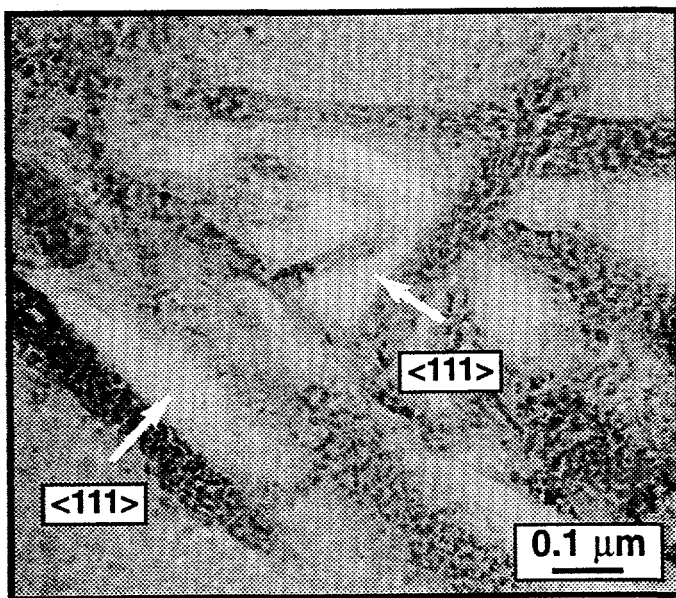


Figure 5. TEM image of acicular CeO_2 grains in the fresh catalyst washcoat.

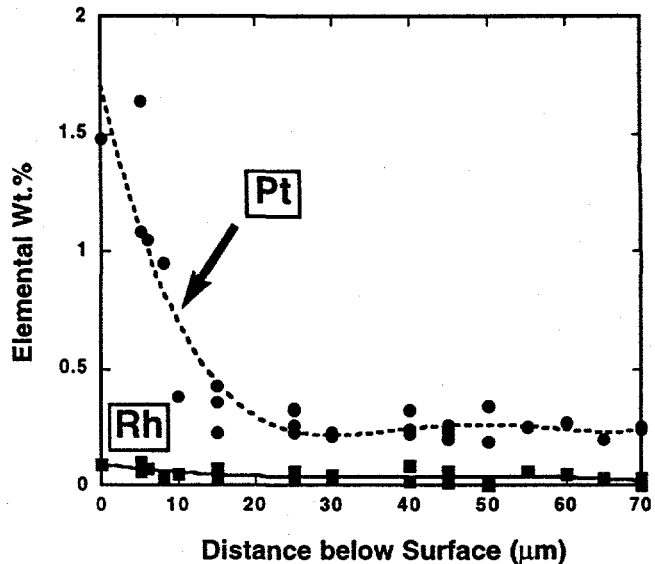


Figure 6. EMPA line profile showing highest concentrations of Pt and Rh were at the washcoat surface.

After the converters were subjected to either the RAT(A)50 or RAT(B)75 test schedules, there was obvious bulk degradation of the washcoat which consisted of large cracks and some weakening of the washcoat/cordierite interface. More importantly, the morphology/structure of all the various washcoat constituents was changed following these aging cycles. On a bulk scale, it was evident that the degree of crystallinity of both the ceria and the γ -alumina was changed after each rapid aging test used, as shown by XRD in Figure 7. This is evidenced by the fact that there is a progressive “sharpening” of the γ -alumina (not as obvious) and ceria (very distinct) peaks in the XRD data which is indicative of an increase in the lattice perfection (reduction of defects/strain) as well as an increase in the crystallite size. Note also that there is a progressive $\gamma \rightarrow \alpha$ -alumina transformation evident in the XRD data, the degree of which is a function of the rapid aging test used. Compared to RAT(B)75, RAT(A)50 provides higher temperatures but a shorter duration of aging. Thus, it is clear from Figure 7 that temperature is a more critical factor than time in determining the stability of the washcoat constituents during aging, since the more substantial changes in the washcoat occur during RAT(A)50.

The XRD data can give an indication of the “structural” changes occurring within the washcoat constituents. However, these data must be compared to actual images of the individual constituents to fully understand the “morphological” changes accompanying the crystallographic changes and the association that these changes have with catalyst deactivation. A TEM image of a CeO_2 agglomerated region after RAT(A)50 is shown in Figure 8. This image shows a distinct rounding of the individual CeO_2 grains compared to the CeO_2

particles in Figure 5. It is also evident that there is a certain degree of sintering occurring between the CeO_2 grains (arrowed in image). Clearly, there is a significant loss of surface area associated with both the morphological change (needle-like particles to more rounded particles) and the associated change in crystallite size. Moreover, the result of CeO_2 particle sintering will further reduce the surface area.

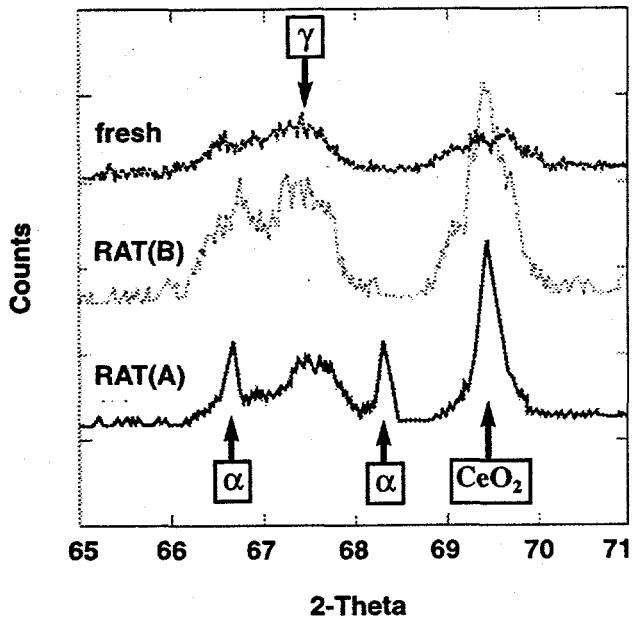


Figure 7. XRD data showing progressive changes in both alumina and ceria crystallinity and crystallite size.

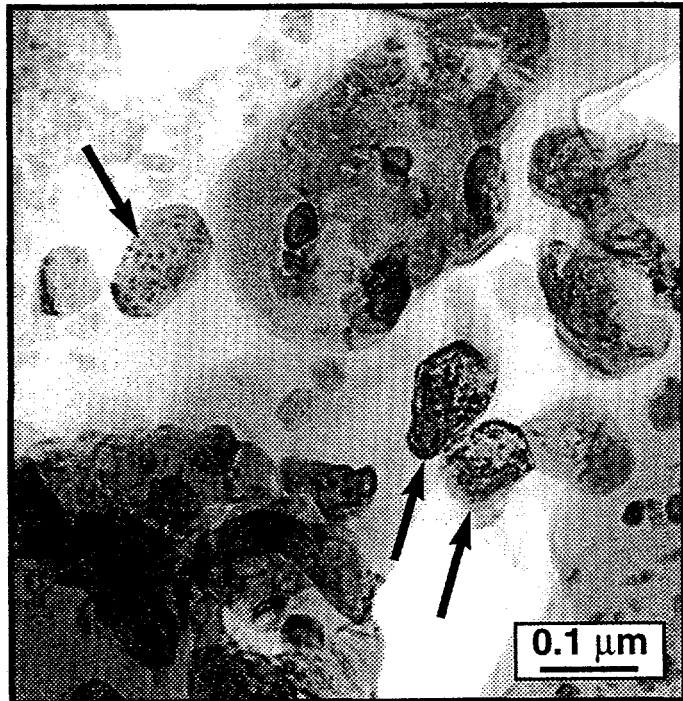


Figure 8. TEM image of the CeO_2 grains after RAT(A)50. Particles exhibit a rounder morphology and have sintered together to form dense agglomerates.

The $\gamma \rightarrow \alpha$ -alumina phase transformation was observed after both RAT(A)50 and RAT(B)75 accelerated test schedules, but was more significant after RAT(A)50 (see Figure 7). The formation of α -alumina is not expected to occur at temperatures less than about 900°C, but can occur rapidly and selectively when short high temperature spikes are reached during an aging cycle or actual engine use. The extent of the $\gamma \rightarrow \alpha$ transformation will affect the performance and lifetime of the catalyst. The α -alumina grains were quite large and easily distinguishable from the γ -alumina regions in the TEM, as shown in Figure 9. There were several unique characteristics of the α -alumina grains formed in the washcoat during aging; (1) the α -alumina crystallite size was large, 0.2-0.6 μm , which is much larger than the γ -alumina crystallite size (<10 nm), (2) the α -alumina grains were extremely well crystallized (as shown by the XRD data), and (3) the α -alumina grains were not randomly distributed within the γ -alumina agglomerates, as one would expect in a $\gamma \rightarrow \alpha$ transformed material, but were present only between the γ -alumina agglomerated regions and in the areas surrounding the CeO_2 crystallites that were located in these regions. It is important to note that the γ -alumina crystallites comprising the large γ -alumina agglomerates were only slightly changed as a result of RAT(A)50 or RAT(B)75. The transformation was limited to the ceria-containing, relatively open regions between the large γ -alumina agglomerates. Thus, not only was there significant grain growth and sintering of the CeO_2 particles, but this was accompanied by the growth of large α -alumina grains within the localized regions where γ -alumina and isolated, fine-grained CeO_2 were in close proximity, and the subsequent encapsulation of many small CeO_2 particles in these regions. Figure 9 illustrates this CeO_2 "encapsulation." There is no evidence in the literature for the identification of this latter effect in other automotive catalysts. Clearly the combination of these "sintering" effects will severely limit the life of a catalyst.

In order to further evaluate the $\gamma \rightarrow \alpha$ -alumina phase transformation in the TWCs, microstructural analysis was performed on catalysts containing varying amounts of ceria (20, 40, and 60 vol.%) subjected to the longer RAT(A)200 test schedule. The performance results for converters subjected to RAT(A)50 and RAT(A)100 have been published previously [15]; it was reported that the HC, CO, and NOx conversions on the sweep tests were maximized when 40% ceria was in the washcoat; however, no microstructural results were presented. Representative SEM images of the 20%, 40%, and 60% ceria-content washcoats after RAT(A)200 are shown in Figures 10, 11, and 12, respectively. These images should be compared to the SEM image of the fresh catalyst washcoat given in Figure 3. The microstructural features which are present in the RAT(A)200 tested washcoat but which are not present in the fresh washcoat are the grey, round features arrowed in Figure 10. These features were identified as α -alumina grains via electron diffraction in the TEM and correspond to the same morphological features described previously

and shown in Figure 9. There are differences in the distributions and amounts of α -alumina between the three washcoats shown in Figures 10-12, differences which are due to both the original ceria content and the original ceria distribution in the washcoat. XRD can be used to quantify the extent of the $\gamma \rightarrow \alpha$ -alumina transformation as a function of ceria content in the washcoat, as shown in Figure 13. The distribution of ceria in the 60% ceria-containing washcoat is much less agglomerated and more homogeneously dispersed as fine particles than in either the 20% or 40% ceria-containing washcoats. The α -alumina has primarily been found within/surrounding the finely dispersed ceria particles between γ -alumina agglomerates. Apparently, the distribution of finer CeO_2 particles, as opposed to the more agglomerated regions, allows for more nucleation of α -alumina in these regions, whereas the agglomerated CeO_2 regions (which were more prevalent in the 20% and 40% ceria-containing washcoats) are not as affected by the $\gamma \rightarrow \alpha$ transformation. Thus, it is probable that the finer distribution of ceria in the 60% content washcoat, as opposed to the more agglomerated ceria regions found in the 20% and 40% washcoats, was more susceptible to the $\gamma \rightarrow \alpha$ transformation (more nucleation sites were available for $\gamma \rightarrow \alpha$); the agglomerated regions in the 20% and 40% ceria washcoats remained essentially unaffected by the transformation. Note from Figure 13 that in the more agglomerated ceria washcoats (20% and 40%), the amount of γ -alumina that transformed to α -alumina was very similar, but when the ceria was more evenly distributed as finer-grained particles in regions between γ -alumina agglomerates (60%), much more γ transformed to α .

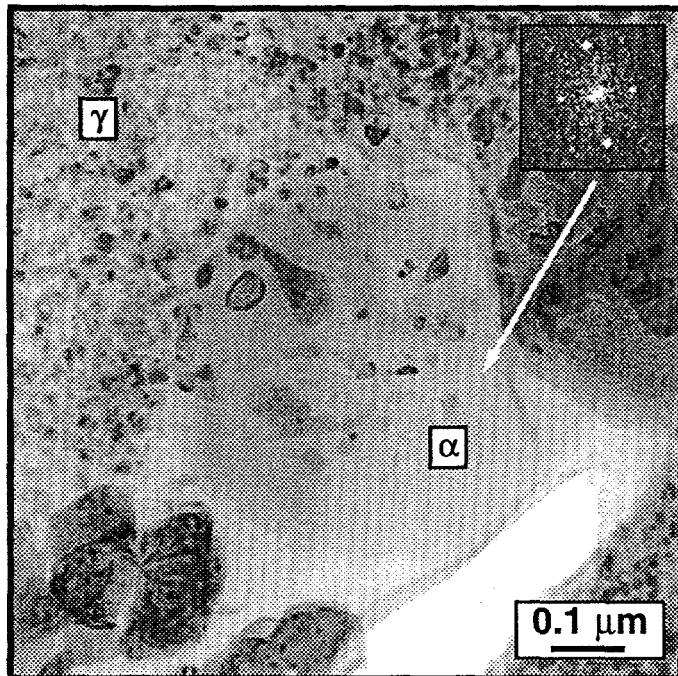


Figure 9. Large α -alumina single-crystal grains were identified between γ -alumina agglomerates by electron diffraction (inset) and surrounded many ceria particles (dark regions encapsulated within α -alumina).

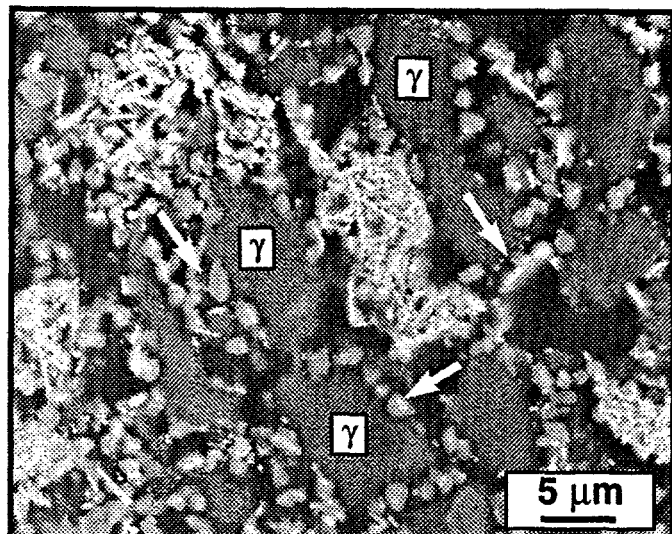


Figure 10. SEM image of the bulk constituent relationships in the 20% ceria-containing washcoat after RAT(A)200. Arrows point to α -alumina grains.

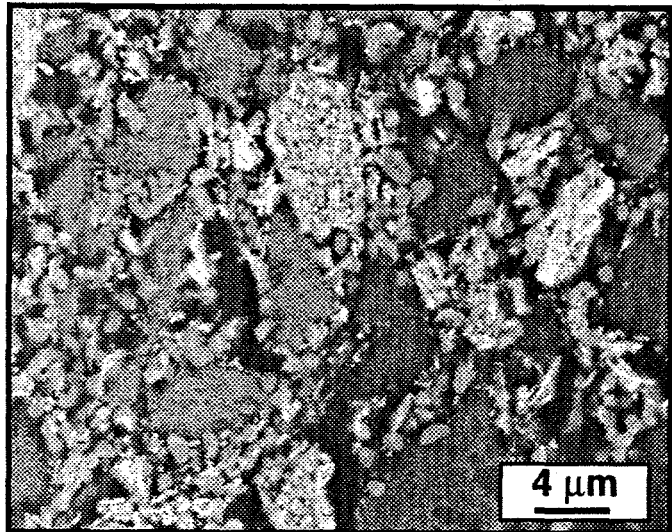


Figure 11. SEM image of the 40% ceria-containing washcoat structure after RAT(A)200.

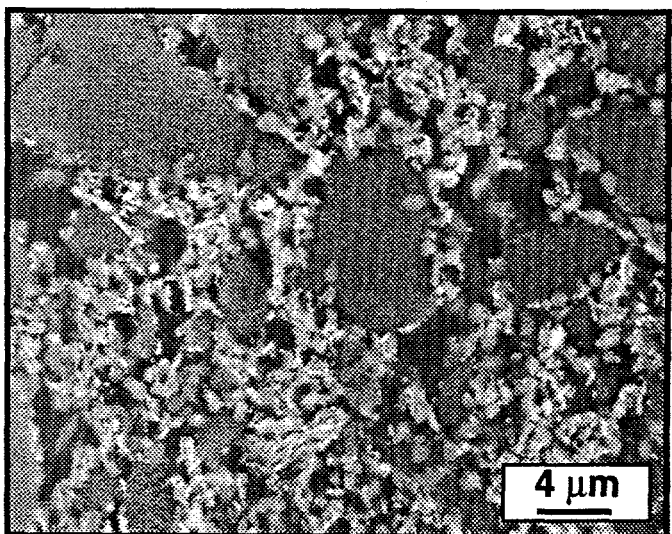


Figure 12. SEM image of the 60% ceria-containing washcoat after RAT(A)200. Note that the ceria is more dispersed between the γ -alumina regions here.

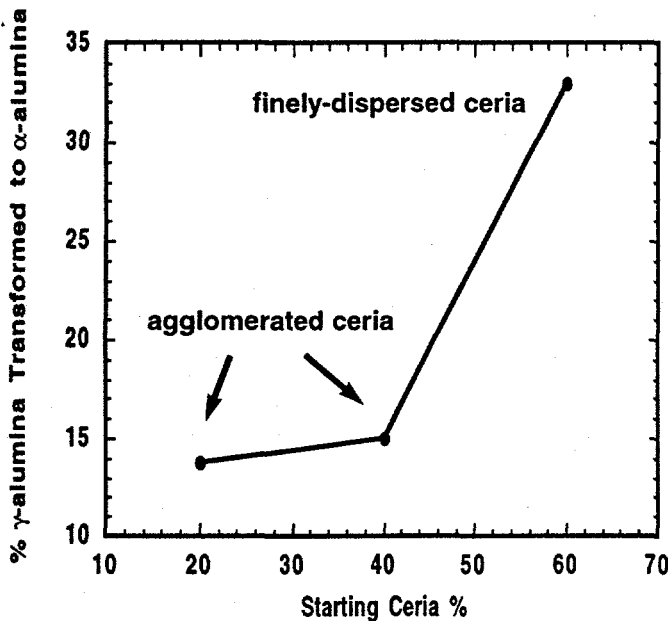


Figure 13. Quantitative XRD showing the relationship between the amount of α -alumina formed during RAT(A)200 and the amount of ceria in fresh catalyst washcoat.

Redistribution of the precious metals in the catalyst washcoat is also expected to occur at normal automobile operating temperatures. In the fresh TWC, both the Pt and Rh are atomically dispersed within the washcoat; no individual Pt or Rh particles were identified. However, the concentrations of both Pt and Rh were higher at the washcoat surface (see Figure 6.) After either RAT(A)50 or RAT(B)75, the distribution changed such that the precious metals were more evenly distributed through the washcoat thickness, as shown in Figure 14. The formation of Pt-Rh alloy particles arising from long-range diffusion of both elements during the aging tests contributed to the observed redistribution. In fact, a bimodal distribution of Pt/Rh particle sizes was observed by TEM, and the measured Pt/Rh ratio was found to change with individual particle size. Figure 15 compares size vs. Pt/Rh weight % ratios for the distribution of larger sized particles only. The average Pt-Rh particle size depended on the aging treatment; the higher the temperature (RAT(A) vs. RAT(B)), the larger the average particle size. Longer test times also resulted in larger particle sizes. As the Pt-Rh particle size increased, the amount of Rh within the particles also increased, which is evidence of increasing Pt-Rh alloying as a function of time and temperature. There was also a distribution of extremely small alloy particles found within the washcoat (1-10 nm in diameter) which had very high Rh contents (Rh-rich) as compared to the much larger particles shown in Figure 15. Composition-size diagrams have been used to understand difference between active and less active catalyst systems. In a study by Lyman, et. al. [17], composition-size diagrams were used to study a variety of Pt-Rh alloy catalysts and it was determined that the Pt-rich particles had higher activities than other particles examined, at least for NO_x

reduction. In the TWC studied here (28% ceria), the bimodal distribution of precious metal particle sizes was observed for all aging cycles studied: extremely small Rh-rich particles and much larger Pt-rich particles. It is always desirable to have a good distribution of extremely small particles of a given composition in order to provide a high surface area of precious metal. However, sintering of the precious metal particles and encapsulation of these particles by other constituents (see Pt-Rh particle "encapsulated" within ceria in Figure 16) as a result of the competing effects of grain growth, sintering, and phase transformation all contribute to the deactivation of the TWC. Stabilization of the washcoat constituents is critical to the preservation of catalyst performance and lifetime.

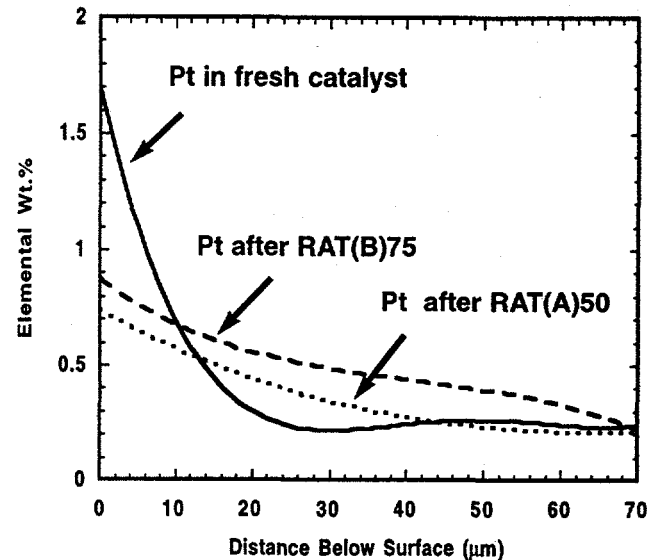


Figure 14. Summary of Pt redistribution as a function of accelerated test schedule.

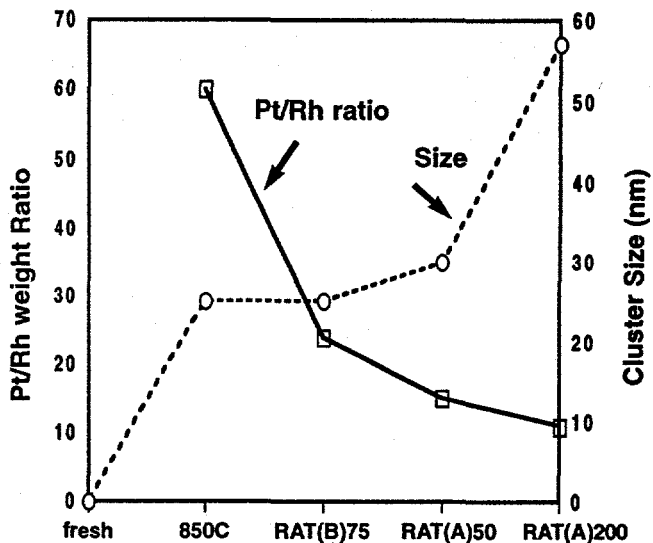


Figure 15. Inverse relationship between Pt/Rh composition and Pt-Rh particle size for catalysts subjected to different test cycles.

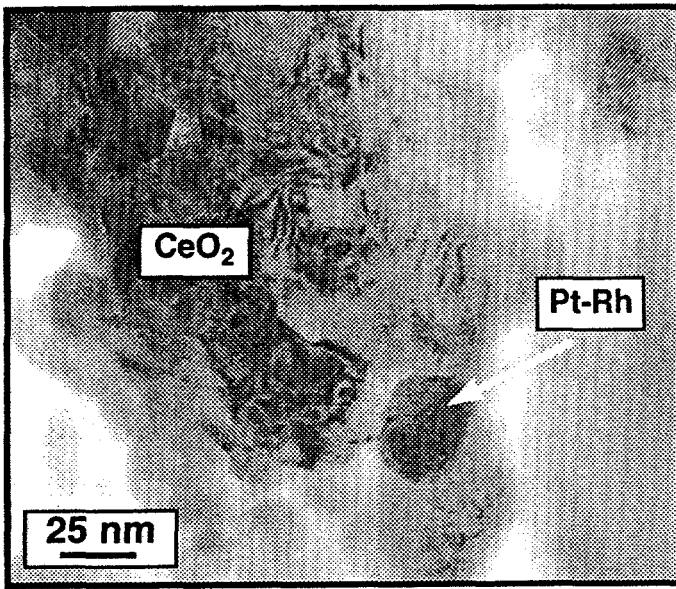


Figure 16. Pt-Rh particle encapsulated in ceria and rendered essentially non-active as a result of competing thermal effects such as grain growth and sintering.

CONCLUSIONS

It has been shown that microstructural characterization is essential for the complete understanding of catalyst deactivation mechanisms. In this study, several microcharacterization techniques have been utilized to understand the thermally induced changes that contribute to the deactivation of a TWC. The main conclusions of this work are:

1. The fresh TWC washcoat consisted of agglomerated regions of fine-grained γ -alumina and ceria. No individual Pt or Rh particles were found in the starting catalyst.
2. EMPA was used to determine that both Pt and Rh concentrations were highest at the washcoat surface in the fresh catalyst.
3. Significant morphological changes and sintering of acicular ceria particles were observed after either RAT(B)75 or RAT(A)50. The higher temperature RAT(A)50 resulted in more significant changes in catalyst washcoat bulk microstructure.
4. A localized $\gamma \rightarrow \alpha$ -alumina phase transformation was observed after either RAT cycle. Large α -alumina grains were identified between γ -alumina agglomerates and surrounded (encapsulated) fine-grained ceria particles within these regions. Large agglomerated ceria regions remained unaffected by the $\gamma \rightarrow \alpha$ transformation.
5. The washcoat containing 60% ceria was most susceptible to $\gamma \rightarrow \alpha$ transformation since the ceria was more finely dispersed than in either 20% or 40% ceria-containing washcoats.

6. Pt-Rh alloy particles formed during the RAT tests. The composition of the individual particles depended on the particle size; extremely small (<10 nm) particles were Rh-rich whereas larger particles (>20 nm) were Pt-rich. The average size of Pt-Rh particles formed depended on the test cycle; larger particles formed during RAT(A) schedule and also for longer times. Increased Rh contents were found in the larger Pt-rich particles after higher temperature aging and longer duration of aging. Redistribution of both Pt and Rh was also observed such that surface loading was less pronounced than in the fresh catalyst.

Thermally-induced microstructural changes can significantly affect the performance of an automotive catalyst, and the extent and contribution of the different mechanisms should be fully understood for different catalyst formulations. With this understanding, thermally stable catalyst constituents, such as rare-earth stabilized alumina, stabilized ceria, etc., can be developed to minimize these effects.

ACKNOWLEDGEMENTS

Research sponsored by (1) the Office of Industrial Technologies, Advanced Industrial Materials Program and (2) the Office of Transportation Technologies, High Temperature Materials Laboratory User Program, U.S. Department of Energy, Assistant Secretary for Energy Efficiency and Renewable Energy, under contract DE-AC05-96OR22464 with Lockheed Martin Energy Research Corp.

REFERENCES

1. Hegedus, L.L. and R.W. McCabe, Catalyst Poisoning, Marcel Dekker, Inc. pub., 1984.
2. Peterson, E.E. and A.T. Bell, Catalyst Deactivation, Marcel Dekker, Inc., pub., 1987.
3. Williamson, W.B., J. Perry, R.L. Goss, H.S. Ghandhi, and R.E. Beason, "Catalyst Deactivation Due to Glaze Formation from Oil-Derived Phosphorous and Zinc," SAE Technical Paper 841406 (1984).
4. Joy, G.C., F.S. Molinaro, and E.H. Homeier, "Influence of Phosphorous on Three-Component Control Catalysts: Catalyst Durability and Characterization Studies," SAE Technical Paper 852099 (1986).
5. Carol, L.A., N.E. Newman, and G.S. Mann, "High Temperature Deactivation of Three-Way Catalyst," SAE Technical Paper 892040 (1989).
6. Stenborn, B., G. Smedler, P.H. Nilsson, S. Lundgren, and G. Wirmark, "Thermal Deactivation of a Three-Way Catalyst: Changes in Structural and Performance Properties," SAE Technical Paper 900273, 1990.
7. Datye, A.K., and D.J. Smith, "The Study of Heterogeneous Catalysts by High Resolution Transmission Electron Microscopy," *Catalysis Review* 34 (1&2) Marcel Dekker, Inc., 129-178 (1992).
8. Bernal, S., F.J. Botana, J.J. Calvino, G.A. Cifredo, J.A. Perez-Omil, and J.M. Pintado, "HREM Study of the

Behavior of a Rh/CeO₂ Catalyst Under High Temperature Reducing and Oxidizing Conditions," *Catalysis Today* 23 Elsevier Science Publishers, Amsterdam, (1995) 219-250.

9. Kim, S., and M.J. D'Aniello, "Analytical Electron Microscopy Study of Two Vehicle-Aged Automotive Exhaust Catalysts Having Dissimilar Activities," *Applied Catalysis* 56 Elsevier Science Publishers, Amsterdam, (1989) 23-43.

10. Kim, S., and M.J. D'Aniello, "Electron Microscopy Study of a Rejuvenated Vehicle-Aged Automotive Exhaust Catalyst," *Applied Catalysis* 56 Elsevier Science Publishers, Amsterdam, (1989) 45-56.

11. Rice, S.B., and M.J. Treacy, "The Art of the Possible: An Overview of Catalyst Specimen Preparation Techniques for TEM Studies," *Materials Research Society Symposium Proceedings* 115 The Materials Research Society, Pittsburgh, PA (1988) 15-27.

12. More, K.L., D.W. Coffey, and T.S. Geer, "Cross-Section TEM Specimen Preparation of Friable Catalyst Materials to Preserve Constituent Spatial Integrity," *Microbeam Analysis - 1995*, E.S. Etz, ed., VCH Publishers, New York (1995) 137-38.

13. Theis, J.R. and W.J. LaBarge, "An Air/Fuel Algorithm to Improve the NO_x Conversion of Copper-Based Catalysts," SAE Technical Paper 922251 (1992).

14. Sims, G.S. and S. Johri, "Catalyst Performance Study Using Taguchi Methods," SAE Technical Paper 922338 (1992).

15. Theis, J.R., W.J. LaBarge, and G.B. Fisher, "The Effects of Catalyst Volume and Ceria Content on the Emission Performance and Oxygen Storage Capacity of Automotive Catalysts," SAE Technical Paper 932666 (1993).

16. Bradley, S.A., M.J. Cohn, and S.J. Pennycook, "Z-Contrast Imaging of Supported Pt and Pd Clusters," *Microscopy Research and Technique* 28 (1994) 427-29.

17. Lyman, C.E., R.E. Lakis, and H.G. Stenger, Jr., "Composition-Size Distribution Diagrams for Alloy Catalysts," in *Microbeam Analysis - 1995*, E.S. Etz, ed., VCH Publishers, New York (1995) 404-405.